Available online at www.sciencedirect.com
SCIENCE DIRECT®
Surface Science 545 (2003) L735–L740
SURFACE SCIENCE
www.elsevier.com/locate/susc

Surface Science Letters

Defect lines and two-domain structure of hexagonal boron nitride films on Ni(1 1 1)

W. Auwärter *, M. Muntwiler, J. Osterwalder, T. Greber

Physik-Institut, Universität Zürich, Winterthurerstrasse 190, CH-8057 Zürich, Switzerland

Received 19 June 2003; accepted for publication 21 August 2003

Abstract

The growth of hexagonal boron nitride (*h*-BN) on Ni(1 1 1) at submonolayer coverages results in triangular islands with two different orientations. In combining X-ray photoelectron diffraction and scanning tunneling microscopy it is demonstrated that these two island types correspond to *fcc* and *hcp* domains of *h*-BN/Ni(1 1 1). The domain boundaries appear as defect lines that are also present in complete *h*-BN monolayers. Based on the experimental data, structural models for the two domains and the defect lines are discussed.

Keywords: Scanning tunneling microscopy; Photoelectron diffraction; Nickel; Boron nitride; Surface defects

1. Introduction

Single monolayers of hexagonal boron nitride (*h*-BN) can be grown on Ni(1 1 1) and form an atomically sharp interface [1,2]. A nonmetallic *h*-BN spacer layer is a model substrate with low surface energy [3] and represents a good candidate to build an ultimately thin metal-insulator-metal structure. Independent low-energy electron diffraction (LEED) [4] and X-ray photoelectron diffraction (XPD) studies [2,5] revealed a structure with a slightly corrugated *h*-BN monolayer: N atoms sit on *top* of every outermost Ni atom, while the B atoms predominantly occupy the *fcc* sites, where, in contrast to the *hcp* site, no Ni atom is right below in the second layer. This experimental result, i.e. the (N, B) = (*top*, *fcc*) structure for the *h*-BN monolayer on Ni(1 1 1), was recently confirmed by a density functional theory (DFT) study [6], which furthermore indicates that a second structure, the (N, B) = (*top*, *hcp*) configuration, is energetically only slightly less favourable (9 meV/BN-unit) than the *fcc* structure. Scanning tunneling microscopy (STM) experiments found a very low density of defect lines in well-prepared *h*-BN films. These defects strongly influence the growth of metals on *h*-BN/Ni(1 1 1) and establish nucleation centers for cluster formation and metal intercalation [3]. Thus they appear to be of importance for the use of *h*-BN as surfactant, for the quality of metal/*h*-BN/Ni(1 1 1) interfaces or for the formation of templates to produce ordered nanostructures on this substrate.

* Corresponding author. Tel.: +41-1-635-66-97; fax: +41-1-635-57-04.
E-mail address: williau@physik.unizh.ch (W. Auwärter).

0039-6028/$ - see front matter © 2003 Elsevier B.V. All rights reserved.
doi:10.1016/j.susc.2003.08.046

This letter reports on the origin of such defect lines in almost perfect *h*-BN/Ni(1 1 1) layers. They are boundaries between *fcc* domains and a minority population of the *hcp* domains. From STM and XPD measurements on submonolayer films with varying *fcc–hcp* domain ratios a structural model for the two domains and the defect lines is derived.

2. Experimental

The XPD patterns were recorded in a modified VG ESCALAB 220 spectrometer [7] using Si Kα ($\hbar\omega = 1740$ eV) radiation while the local real space surface structure was imaged by a Park Scientific Instruments VPII STM. A low vibrational noise coupling between the spectrometer and the STM chamber allows for sample transfer under UHV conditions and thus to perform photoelectron spectroscopy and atomic resolution STM measurements on the very same surface. All STM data were recorded at room temperature using electrochemically etched tungsten tips. The dI/dV conductivity maps were taken simultaneously with constant-current topographic images by modulating the sample bias V ($\Delta V = 40$ meV) at a frequency of about 5 kHz while detecting the current variations by a lock-in amplifier. After cleaning the Ni(1 1 1) single crystal by cycles of 800 eV Ar^+ sputtering followed by an optional oxygen exposure (see below) and annealing to 1000 K, submonolayer coverages Θ ($0.2 \leqslant \Theta \leqslant 0.4$) of *h*-BN were prepared by dosing about 0.2 L of borazine $(HBNH)_3$ while the Ni(1 1 1) substrate was kept at 1070 K. A more detailed description of the experimental apparatus and sample preparation procedures can be found in our previous publications [2,3,8].

3. Results and discussion

To understand the origin of the linear defects in *h*-BN monolayers, it is useful to study incomplete *h*-BN monolayers with higher defect concentrations. Fig. 1 shows a constant current STM image of the Ni(1 1 1) surface, partially covered with *h*-BN islands. Two different orientations of triangular shaped islands are observed on the same Ni terrace. In comparison to a substrate step the apparent island height (as expressed by the gray scale) is reduced due to a lower density of states in the *h*-BN [6]. We will not further address this effect, but exploit it later in the conductivity imaging mode of STM. The crucial point is the appearance

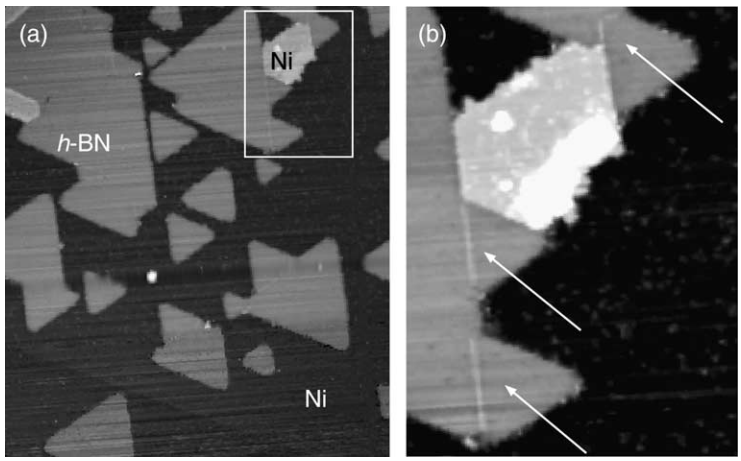

Fig. 1. (a) STM image of the Ni substrate partially covered by triangular *h*-BN islands. Defect lines are found where two oppositely oriented triangles meet (0.31 μm × 0.36 μm, $I = 1$ nA, $V = -0.2$ V). (b) Enlarged image of the area marked in (a) with arrows pointing to the defect lines.

of linear defects where triangles of opposite orientations touch (see Fig. 1(b)). Thus, the defect lines are linked to the two island species. For the following reasons, we argue that the island shapes are determined by steps exhibiting a specific well-defined arrangement of the B and N atoms relative to the Ni top layer: (i) the island perimeter is not hexagonal and (ii) kinetic effects [9,10] can be excluded as origin for the two triangle orientations since the temperature was kept constant during preparation. A similar situation is known from faulted (involving a stacking fault) and unfaulted triangular Co islands on Cu(1 1 1) [11,12]. The stable step geometry must be the same for both triangle orientations, which immediately invokes a different registry between the *h*-BN lattice and the Ni substrate for the two island species.

Fig. 2 shows that this is indeed the case. It is based on two sample preparations (P_1, P_2) that have been intentionally grown with a different ratio between the two island types (see below). Information about the average internal island structure is gained from XPD. Fig. 2(a) represents a Si Kα excited B 1s diffractogram recorded from sample P_1 in the interesting range of the polar emission angle θ ($86° > \theta > 78°$) which contains the information on the average position of the N atoms relative to the B atoms. We find three dominating intensity maxima in the $\langle \bar{1}\,\bar{1}\,2 \rangle$ directions. As discussed in Ref. [2] this pattern is produced by forward scattering along the B–N axis and indicates a predominant *h*-BN domain with the N atoms positioned on *top* of the outermost Ni atoms and the B atoms on the *fcc* sites. A STM image for the same preparation P_1 is displayed in Fig. 2(b). It is taken in the conductivity mode to facilitate the discrimination of *h*-BN patches (black areas) from the bare Ni (white areas) and

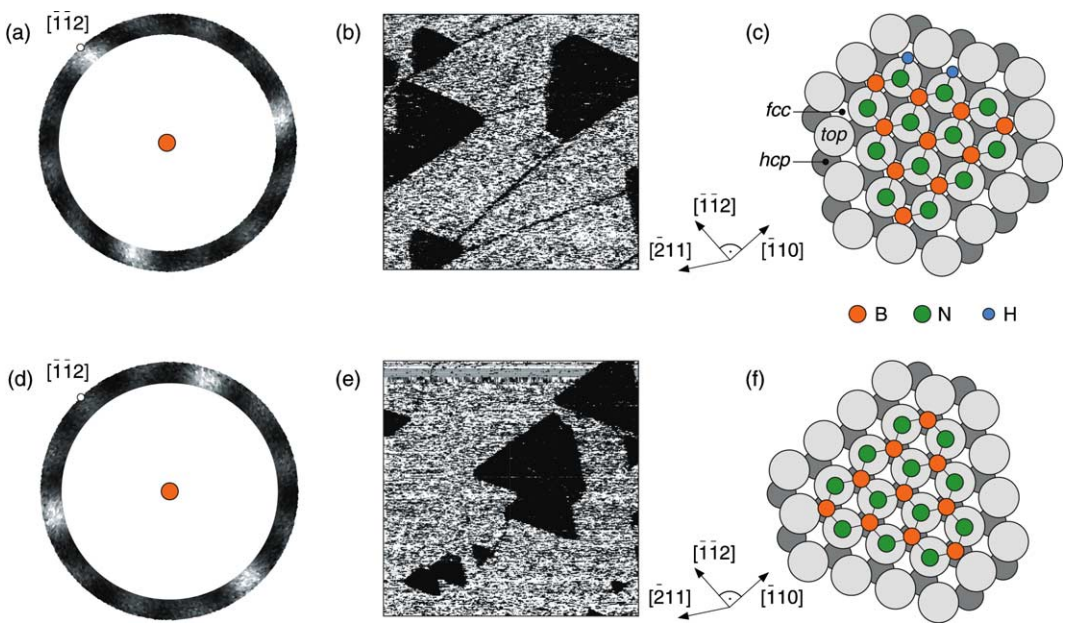

Fig. 2. XPD and STM results on *h*-BN islands partially covering the Ni substrate for preparation P_1 (a–c) and P_2 (d–e): (a) Si Kα excited B 1s XPD pattern. The threefold maxima coincide with the $[\bar{1}\,\bar{1}\,2]$ directions. (b) Corresponding STM conductivity image (0.4 μm × 0.4 μm, $I = 1$ nA, $V = -0.8$ V). The *h*-BN triangles (black) point towards $[\bar{1}\,\bar{1}\,2]$ (the dark lines represent steps which induce a slight contrast). (c) Top view of a model representing the island structure in (b) and (a): the configuration is (N, B) = (*top*, *fcc*). The small atoms indicate the possible existence of hydrogen at the step edges. (d) Si Kα excited B 1s XPD pattern. The main maxima point towards the $[\bar{2}\,1\,1]$ direction. (e) Corresponding STM conductivity image (0.4 μm × 0.4 μm, $I = 3$ nA, $V = -0.6$ V). The *h*-BN triangles (black) are oriented towards $[\bar{2}\,1\,1]$. (f) Top view of a model representing the island structure in (e): the configuration is (N, B) = (*top*, *hcp*).

shows *h*-BN triangles pointing in the $[\bar{1}\,\bar{1}\,2]$ direction. These data combined lead to the model for the triangles displayed in Fig. 2(c). It bases on the structure of the *fcc h*-BN monolayer ((N, B) = (*top*, *fcc*)). The island boundaries are speculatively terminated by N atoms. As the STM experiment gives only the directions of the edges, there is no direct proof for N termination. However, a B termination of the triangles would result in incomplete BN hexagons and thus lead to more unsaturated bonds. We furthermore expect that the open N bonds at the island edges are saturated by H atoms.

The results of a second preparation P_2 are displayed in Fig. 2(d) and (e). Surprisingly, the B 1s XPD pattern in Fig. 2(d) is rotated by 60° relative to the one in Fig. 2(a), [1] but is otherwise identical. This finding stands for *h*-BN domains where the nearest neighbor B–N directions point along $\langle\bar{2}\,1\,1\rangle$. The corresponding STM image (Fig. 2(e)) is indeed dominated by *h*-BN triangles pointing in the $[\bar{2}\,1\,1]$ direction. Thus, they are rotated as well by 60° with respect to the *fcc* islands of Fig. 2(b). The threefold XPD pattern of the *h*-BN triangles in Fig. 2(d) is in principle consistent with three adsorption geometries: (N, B) ∈ {(*hcp*, *fcc*), (*top*, *hcp*), (*fcc*, *top*)}. However, it follows from the earlier discussion that, if the *rotated* triangles have an edge structure similar to the *fcc* ones, the only possible configuration is (N, B) = (*top*, *hcp*). This *hcp* configuration is the only geometry predicted by DFT to be stable apart from the *fcc* arrangement [6]. The resulting structural model is shown in Fig. 2(f).

These results strongly suggest that the orientation of the triangles is directly related to their atomic structure. This is quantified for three preparations (P_1, P_2, P_3). Up to 50 STM images taken at different positions containing several hundreds of islands were evaluated. The coverages resulting from the sum of all triangle-areas nicely agree with the corresponding *h*-BN coverages as determined by focussed Al Kα excited XPS. This ensures that our identification of the *h*-BN triangles is correct and that STM and photoemission measurements can be directly compared. To quantify the information contained in the STM data, we determine the ratio α_{STM} defined as follows:

$$\alpha_{\mathrm{STM}} = \frac{\sum A_{fcc}}{\sum A_{fcc} + \sum A_{hcp}}.$$

A stands for the area of a *h*-BN triangle. The label *fcc* is attributed to the triangle species pointing towards $[\bar{1}\,\bar{1}\,2]$, while *hcp* refers to the triangle type oriented towards $[\bar{2}\,1\,1]$. Thus the ratio α_{STM} describes the contribution of all *fcc* triangles to the entire *h*-BN coverage. In Fig. 3 the α_{STM} values obtained for three preparations are plotted vs. the coverages Θ as determined by STM. The XPD patterns in Fig. 2(a) and (d) tell us that two *h*-BN unit cell orientations exist. The pattern of a mixed-phase sample is a linear combination of the pure *fcc* and *hcp* case. To analyze the measured patterns we compare them to diffraction patterns from single scattering cluster calculations (SSC), which base on a single *h*-BN domain [2]. An azimuthal cut at $\theta = 82°$ in the experimental diffraction pattern is fitted by a combination of azimuthal cuts for the *fcc* and *hcp* domains:

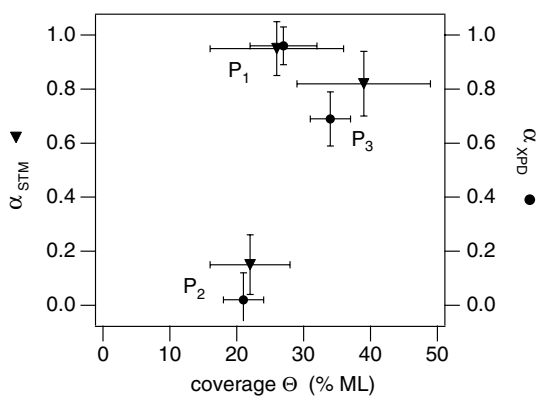

Fig. 3. Comparison of XPD (solid circles) and STM (solid triangles) results on *h*-BN islands for three preparations (P_1–P_3): The concentrations α_{STM} of *fcc* triangles and the coverages determined by STM agree well with the corresponding values from XPD. Note that the actual value of α is not a function of the coverage but is solely dependent on the preparation (see text).

[1] The absolute orientation of the B 1s XPD patterns was determined from the Ni 2p substrate XPD pattern that shows a three-fold symmetry.

$$I_{\mathrm{exp}}(\theta,\phi) \propto \alpha_{\mathrm{XPD}} I_{\mathrm{SSC}\,fcc}(\theta,\phi) + (1-\alpha_{\mathrm{XPD}}) I_{\mathrm{SSC}\,hcp}(\theta,\phi) \quad (1)$$

The resulting parameter α_{XPD} describes the contribution of the original (N, B) = (*top*, *fcc*) domain to the diffraction pattern and should correspond to α_{STM}. α_{XPD} and α_{STM} are compared in Fig. 3. The plot verifies an unambiguous correlation between the orientation of the *h*-BN lattice and the triangle direction.

With this information we come closer to an atomic understanding of the defect lines. Fig. 4 sketches a situation as found for example in Fig. 1(b). Where two islands of opposite orientation merge, the structural models of Fig. 2(c) and (f) give an explanation for the defect lines. As the two islands grow from two remote seeds, the separation in between decreases up to a critical spacing. A defect-free merging of the two *h*-BN patches is not possible due to the different registry to the substrate. Thus a linear imperfection separates the *h*-BN domains. The detailed geometric and chemical structure of the defect lines can not be deduced from our experiment: As indicated in the bottom part of Fig. 4 a hydrogen saturation of the island boundaries leads to a more open defect than a bare nitrogen termination. However, the direction of the defect lines teaches us that the *h*-BN growth proceeds via *fragments* of BN six-rings. An assembly of *h*-BN islands from unbroken molecules would result in defect lines rotated 30° away from the observed directions. Possible reaction and growth mechanisms for *h*-BN formation are further discussed elsewhere [8]. The observed imaging of defect lines as either weak protrusions or depressions by STM may be explained by the reactivity of these defects that make them a preferred location for adsorption.

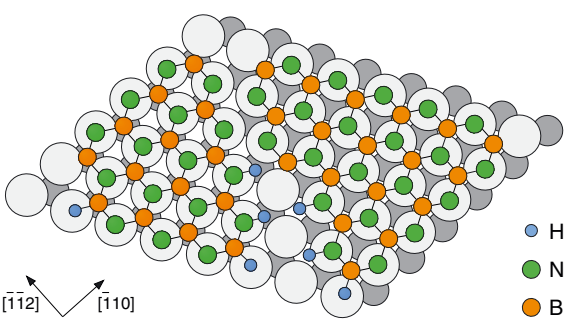

Fig. 4. Structure model of a defect line in *h*-BN/Ni(1 1 1): two *h*-BN islands of inequivalent domains can not merge without defect because of their different registry to the substrate. An island terminated by nitrogen results in a defect structure as seen in the top part. No space for further BN adsorption is left in between the two patches. Hydrogen saturated island edges (bottom part) would produce a more open defect line.

The origin and control of the *fcc*-*hcp* domain ratio α is not fully understood. Two-domain structures were observed for all investigated *h*-BN coverages ($0.1 \leqslant \Theta \leqslant 1$). α critically depends on the sample preparation prior to borazine exposure and on the status of the borazine that is known to slowly degrade at room temperature. *All* XPD measurements on *h*-BN ($\Theta \leqslant 1$) grown with fresh borazine on a Ni(1 1 1) substrate after oxygen treatment show a threefold pattern corresponding to an overwhelming contribution ($\alpha \geqslant 0.95$) of the (N, B) = (*top*, *fcc*) domain. However, the STM is able to detect a low density of defect lines and thus small areas of the *hcp* domain. O_2 exposure (30 L) of the Ni sample prior to annealing helps e.g. to remove small carbon contaminations in the 1% ML range. This is a hint that smallest amounts of carbon might be key players to control the *fcc–hcp* domain ratio, and thus the density of linear defects.

4. Conclusions

In combining XPD and STM we have demonstrated that two *h*-BN domains, differing in the B adsorption sites (*fcc* or *hcp*), can coexist on Ni(1 1 1). Their area ratio sensitively depends on the initial preparation of the substrate and the borazine. Linear defects mark the boundaries between the two domains. Possible structural models of these line defects were proposed from the presented experiments.

Acknowledgements

We are grateful to H. Sachdev for the production of borazine. This work was supported by the Swiss National Science Foundation.

References

[1] A. Nagashima, N. Tejima, Y. Gamou, T. Kawai, C. Oshima, Phys. Rev. B 51 (1995) 4606.
[2] W. Auwärter, T.J. Kreutz, T. Greber, J. Osterwalder, Surf. Sci. 429 (1999) 229.
[3] W. Auwärter, M. Muntwiler, T. Greber, J. Osterwalder, Surf. Sci. 511 (2002) 379.
[4] Y. Gamou, M. Terai, A. Nagashima, C. Oshima, Sci. Rep. RITU A 44 (1997) 211.
[5] M. Muntwiler, W. Auwärter, F. Baumberger, M. Hoesch, T. Greber, J. Osterwalder, Surf. Sci. 472 (2001) 125.
[6] G.B. Grad, P. Blaha, K. Schwarz, W. Auwärter, T. Greber, Phys. Rev. B 68 (2003) 085404.
[7] T. Greber, O. Raetzo, T.J. Kreutz, P. Schwaller, W. Deichmann, E. Wetli, J. Osterwalder, Rev. Sci. Instrum. 68 (1997) 4549.
[8] W. Auwärter, H.U. Suter, H. Sachdev, T. Greber, submitted.
[9] T. Michely, M. Hohage, M. Bott, G. Comsa, Phys. Rev. Lett. 70 (1993) 3943.
[10] S. Liu, Z. Zhang, G. Comsa, H. Metiu, Phys. Rev. Lett. 71 (1993) 2967.
[11] J. de la Figuera, J.E. Prieto, C. Ocal, R. Miranda, Phys. Rev. B 47 (1993) 13043.
[12] A.L. Vázquez de Parga, F.J. García-Vidal, R. Miranda, Phys. Rev. Lett. 85 (2000) 4365.